Metabolomics (2016) 12:23
DOI 10.1007/s11306-015-0928-y

ORIGINAL ARTICLE

# Effects of synthetic large-scale genome reduction on metabolism and metabolic preferences in a nutritionally complex environment

**Fan Fei[1] · George C. diCenzo[2] · Dawn M. E. Bowdish[3] · Brian E. McCarry[1] · Turlough M. Finan[2]**

Received: 18 May 2015 / Accepted: 10 October 2015


**Abstract** The soil bacterium *Sinorhizobium meliloti* forms nodules on the roots of leguminous plants, where $N_2$ is reduced to ammonia. Its genome includes a 3.65 Mb chromosome, a 1.35 Mb pSymA megaplasmid, and a 1.68 Mb pSymB chromid. pSymA and pSymB constitute ~45 % of the genome and here a non-targeted approach was used to identify the metabolic consequences of the removal of these replicons. Polar and non-polar metabolites from wild-type, ΔpSymA, ΔpSymB, and ΔpSymAB cells and supernatants across a growth curve were analyzed by LC–HILIC–TOF–MS. 2008 metabolite features were identified in the extracellular metabolome of cells grown in LBmc containing yeast extract and casein hydrolysate. 1474 features were found from the intracellular metabolites of cells grown in minimal M9-sucrose medium. Analysis revealed both time and genotype influenced the metabolome, with the removal of pSymB having a much greater effect than the loss of pSymA. Strains lacking pSymB showed an increase in sugar, amino acid, and nucleotide metabolites in the intracellular metabolome, and the loss of pSymB clearly impaired the cell's ability to catabolize exogenous amino acids. We conclude that despite the ability of wild-type, ΔpSymA, ΔpSymB, and ΔpSymAB strains to grow in both M9-sucrose and LBmc media, the removal of pSymA, and particularly pSymB, had clear and dramatic effects on the *S. meliloti* metabolome. The larger effect associated with the pSymB chromid is consistent with the large number of metabolic genes on this replicon and the greater genetic and metabolic integration of this replicon with the *S. meliloti* chromosome.

**Keywords** *Sinorhizobium* · Metabolism · Multipartite · Microbial

## 1 Introduction

Historically, bacteria were thought to have the majority of their DNA present on a single, circular chromosome (Krawiec and Riley 1990). However, in recent years it has become evident that this simplistic view is not generally applicable. A minority of bacteria are said to contain a multipartite genome, where the genome is divided into multiple large pieces, known as replicons (Harrison et al. 2010). This type of genome organization is present in a number of organisms of societal consequence, including plant symbionts (e.g. *Rhizobium* and *Sinorhizobium*), plant pathogens (e.g. *Agrobacterium*), and animal and human pathogens (e.g. *Vibrio*, *Burkholderia*, and *Brucella*) (Harrison et al. 2010). By gaining an understanding of the evolution and functional significance of the multipartite genome, we hope to gain generalizable insight into the biology of these organisms.

Fan Fei and George C. diCenzo have contributed equally to this work.

**Electronic supplementary material** The online version of this article (doi:10.1007/s11306-015-0928-y) contains supplementary material, which is available to authorized users.

✉ Turlough M. Finan
finan@mcmaster.ca

[1] Department of Chemistry and Chemical Biology, McMaster University, 1280 Main St. W., Hamilton, ON L8S 4M1, Canada

[2] Department of Biology, McMaster University, 1280 Main St. W., Hamilton, ON L8S 4K1, Canada

[3] Department of Pathology and Molecular Medicine, Michael G. DeGroote Institute for Infectious Disease Research, McMaster University, 1280 Main St. W., Hamilton, ON L8N 3Z5, Canada

Published online: 31 December 2015

The Gram-negative α-proteobacterium *Sinorhizobium meliloti* has a multipartite genome and this organism enters into a $N_2$-fixing endosymbiotic relationship with several legumes (Galibert et al. 2001). This agriculturally important process provides the legume host with a source of nitrogen, allowing the plant to grow in nitrogen poor soils. The genome of the model strain Rm1021 (Rm2011) includes a 3.65 megabase (Mb) chromosome, a 1.68 Mb chromid (pSymB), and a 1.35 Mb megaplasmid (pSymA) (Galibert et al. 2001; Sallet et al. 2013). Due in part to the ease with which it can be grown and genetically manipulated, *S. meliloti* has become a model organism for the study of many topics, including $N_2$-fixing symbiosis, carbon metabolism, and the evolution and function of the bacterial multipartite genome (Finan et al. 2002; Galardini et al. 2013; Geddes and Oresnik 2014). Recently, a *S. meliloti* Rm2011 derivative was reported that completely lacks the pSymA and pSymB replicons, a 45 % reduction of the genome (diCenzo et al. 2014). This strain presents an opportunity to employ novel experimental approaches to study the role of the bacterial multipartite genome.

Metabolomics as an approach to study the biology of *S. meliloti* is well established. Studies have effectively used metabolic profiling to examine how the metabolome of *S. meliloti* is influenced by several factors, including carbon source, specific growth rate, and amino acid auxotrophy (Barsch et al. 2004; Keum et al. 2008; Ong and Lin 2003). In addition to the study of free-living *S. meliloti*, metabolic analysis has been employed in the characterization of the *S. meliloti*—legume symbiosis (Barsch et al. 2006; Gemperline et al. 2015; Ye et al. 2013), and in silico analysis has been used to model the metabolism of *S. meliloti* during symbiosis (Zhao et al. 2012). However, to date, the relative contribution of the pSymA and pSymB replicons to the metabolism of *S. meliloti* has not been examined.

Here, we performed a metabolic analysis of the endo- and exo-metabolome of *S. meliloti* using HILIC–TOF–MS. The primary objective of this work was to examine how, if at all, pSymA and pSymB have been integrated into the metabolism of *S. meliloti*, which in turn will provide insight into the biology of *S. meliloti*, and general knowledge of the functional significance of secondary replicons in bacterial genomes. As a secondary objective, we wished to establish HILIC–TOF–MS as a suitable technique for monitoring the metabolic capacity and metabolic preferences of a bacterial population grown in a nutritionally complex environment.

## 2 Materials and methods

### 2.1 Chemicals

HPLC grade methanol (MeOH), ethanol (EtOH), acetonitrile (ACN), chloroform, water and formic acid used for bacterial extraction and LC–MS analyses were purchased from Caledon Laboratories (Georgetown, ON, Canada). Ammonium acetate was purchased from Fisher Scientific Company (Fairlawn, NJ, USA). L-methionine-$d_3$ (98 %), L-tryptophan-$d_5$ (98 %), L-phenylalanine-$d_8$ (98 %), diphenylalanine (phe–phe), and glycine-phenylalanine (gly-phe) were purchased from Cambridge Isotope Laboratories (Landover, MA, USA) for recovery determination (RS) and peak intensity normalization (IS).

### 2.2 Media, strains, and growth conditions

LBmc (per litre: 10 g Bacto tryptone, 5 g Bacto yeast extract, 5 g NaCl, 2.5 mM $MgSO_4$, 2.5 mM $CaCl_2$, 2 μM $CoCl_2$) was used as the complex medium, and M9 (41 mM $Na_2HPO_4$, 22 mM $KH_2PO_4$, 8.6 mM NaCl, 18.7 mM $NH_4Cl$, 4.1 μM biotin, 42 nM $CoCl_2$, 1 mM $MgSO_4$, 0.25 mM $CaCl_2$, 38 μM $FeCl_3$, 5 μM thiamine-HCl, and 10 mM sucrose) was used as the minimal medium. The four *S. meliloti* strains used in this study were described elsewhere (diCenzo et al. 2014; Oresnik et al. 2000). These included the wild-type Rm2011 (SU47 *str-3*), and Rm2011 derivatives lacking pSymA (termed SmA818, or ΔpSymA), pSymB (termed RmP3009, or ΔpSymB), or both (termed RmP2917, or ΔpSymAB). Strains with pSymA or pSymB removed lack all genes on these replicons, with the exception of the $tRNA^{arg}$ and the *smb20996-engA* operon which were integrated into the chromosome as the tRNA and *engA* are essential (diCenzo et al. 2013).

Strains were grown to early stationary phase in 5 mL of M9 or LBmc at 30 °C. The equivalent of 3.0 $OD_{600}$ units per culture were pelleted, washed once with fresh media (M9 or LBmc as appropriate) and resuspended in 1 mL of fresh media. Cultures were diluted in 40 mL to an $OD_{600}$ of 0.05 in the same medium. 5 mL was aliquoted into seven test tubes per sample and grown at 30 °C; cells were harvested from six of the test tubes, and growth of the cultures was monitored using the seventh tube.

### 2.3 Sample collection and extraction

For intracellular metabolic analyses, samples cultured in M9 were collected in sextuple at $OD_{600}$ values of approximately 0.3, 0.5, 0.9, 1.6, and 3.5 (except for Rm2011 which reached ~4.8). Sample sizes of 1000, 600, 300, 176, and 100 μL were taken at each time point, respectively, such that ca. $6 \times 10^8$ cells were collected in each sample. These samples are referred to as M1–5 with M1–4 representing exponential phase, and M5 referencing to stationary phase (Fig. 1a). Cells were pelleted by centrifugation at 4 °C, washed once with saline (0.85 % NaCl), pelleted, and the supernatant carefully removed. Pellets were resuspended and lysed in 2:2:1 MeOH/EtOH/$H_2O$, dried under nitrogen,

and resolubilized in 60 % ACN with IS (Fei et al. 2014) within a week of sample harvesting, with the samples stored at -80 °C between extraction steps. Extracted sample were stored at -80 °C until LCMS analysis, which was completed within one month.

For analysis of the extracellular metabolome, 200 µL of culture grown in LBmc was collected in sextuple at mid-exponential growth (L1), early stationary phase (L2), and late stationary phase (L3) (Fig. 1b). Cells were pelleted by centrifugation at 4 °C, and 20 µL of the supernatant was transferred to a new tube and stored at −80 °C. Within a week, samples were diluted ten-fold in 1:1 MeOH/EtOH containing IS and RS, and stored at -80 °C until LCMS analyses, which was completed within 2 months. Sextuple samples of uninoculated LBmc medium were also collected at 0 (L1LB) and 45 h (L3LB) of incubation at 30 °C as experimental controls.

Two independent sets of pooled samples for both the intracellular and extracellular metabolome were prepared by combining 5 µL of all corresponding samples.

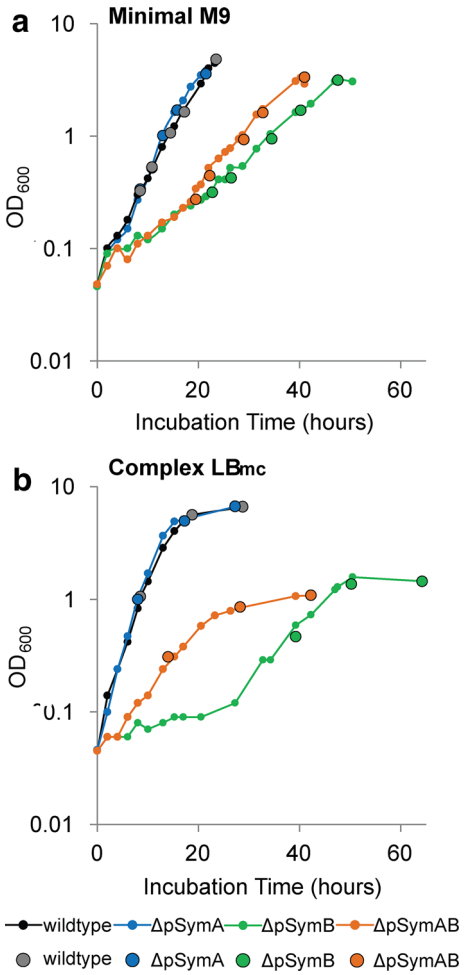


**Fig. 1** Growth curves of *S. meliloti* wild-type, ΔpSymA, ΔpSymB and ΔpSymAB strains in **a** M9 minimal medium containing 10 mM sucrose and **b** LBmc medium. The *small solid circles* represent $OD_{600}$ readings from a fixed sample of each strain throughout the entire growth curve. Samples were removed from culture tubes throughout growth and prepared for metabolomic analysis. The *large solid circles* with a *black border* indicate the average $OD_{600}$ readings of the quintuplicate or sextuplicate samples collected for intracellular and extracellular metabolomic analyses. *Black* wild type; *blue* ΔpSymA; *green* ΔpSymB; *orange* ΔpSymAB (Color figure online)

## 2.4 HILIC–TOF–MS analyses

The intracellular and extracellular extracts were analyzed in two separate batches using an Agilent Technologies 1200 RR Series II liquid chromatograph (LC) coupled to a Bruker MicrOTOF II Mass Spectrometer (Fei et al. 2014). An injection of 2 µL was separated on a 50 mm × 2.1 mm Kinetic 2.6 µm HILIC column of pore size of 100 Å (Phenomenex, CA, USA). The mobile phases were HPLC grade acetonitrile (A) and 10 mM ammonium acetate in HPLC grade water adjusted to pH 3 with formic acid (B) at a flow rate of 200 µL/min. The column temperature was maintained at 40 °C, and the auto sampler storage tray was set at 4 °C. The mobile phase gradient eluted isocratically with 95 % ACN for 0.5 min followed by a gradient to 35 % ACN over 12 min. The gradient system was maintained at 35 % ACN for 0.5 min and returned to 95 % ACN over 1 min. The gradient was then followed by a 10 min re-equilibration phase prior to the next injection. The total time for the HILIC gradient was 24 min for both ESI+ and ESI− modes. Injections operating in the positive ionization mode or the negative ionization mode were performed in separate runs. The MS settings were identical to those previously described (Fei et al. 2014).

Pooled samples were injected seven times at the beginning of the analyses to condition the column, and again after every five samples. A total of 31 and 26 pooled samples were run for intra- and extracellular samples, respectively. A methanol blank and a standard mixture containing all IS and RS were also run for every 10 samples. A total of 82 extracellular extracts and 115 intracellular extracts were run in random order once but in both ESI- and ESI + modes.

## 2.5 Data processing and metabolite identification

For the data processing and analyses (Fei et al. 2014), the LC–MS data files were converted to the .mzXML format using Bruker CompassXport following internal calibration with intracellular sodium formate cluster ions using Bruker's DataAnalysis 4.0 SP4. The metabolic features were extracted and aligned using open source XCMS with centWave algorithm (Smith et al. 2006); adducts, isotopic ions, and in-source fragments were identified using CAMERA (Kuhl et al. 2012).

Metabolite features with an apparent retention factor $k_{app}$ lower than 0.7 were removed as well as isotopic ions,

features corresponding to IS, RS, and sodium formate clusters. For the extracellular metabolome, the region of retention from 7.0 to 7.8 min were excluded from the data matrix due to ion suppression. The peak areas of intracellular metabolite features were normalized to IS and $OD_{600}$; the peak areas of all extracellular metabolic features were only normalized to IS. Features with greater than 20 % variance in the pooled sample were removed to obtain the final metabolite feature list (Dunn et al. 2011).

Metabolite features were identified by matching the *m/z* and retention value to those of the available authentic standards or matches to MS/MS fragment pattern on Metlin (Smith et al. 2005). The MS/MS was performed on a ThermoScientific Dionex Ultimate 3000 rapid separation LC coupled to Bruker maXis 4G QTOF MS using a modified LC–HILIC–MS method, and detailed procedures can be found in Online Resource 1.

### 2.6 Statistical analyses

Both intracellular and extracellular metabolic data were analyzed using Umetrics SIMCA-P+ 12 software (Umeå, Sweden). Pareto scaling was applied prior to principal component analysis (PCA) and to orthogonal partial least-squares discriminative analysis (OPLS-DA). OPLS-DA was used to differentiate metabolite profiles between different strains and growth phases. The model validation parameters $R^2X$, $R^2Y$, and $Q^2$ were used to assess the fitness of the model. $R^2X$ ($R^2Y$) indicated the fraction of the metabolite features (X) and treatment (Y) matrix that was explained by the model. A prediction statistic ($Q^2$) above 0.4 was indicative of a robust model, i.e. true differences between the comparing groups, and $Q^2$ between 0.7 and 1.0 indicated the model was highly robust (Jonas et al. 2008). Both $R^2$ and $Q^2$ followed an upward trend from 0 to 1. For an over fit model, $R^2$ approached 1, and $Q^2$ fell towards 0.

Between subjects two-way ANOVA and hierarchical cluster analysis (HCA) were computed and plotted using MetaboAnalyst 3.0 (Xia et al. 2015). Heatmaps were plotted using R 2.12.2 and RStudio 0.98.501. Between subjects two-way ANOVA with p less than 0.01 with a Bonferroni correction were used to identify metabolite features that were significantly different between strains and growth phases. HCA and heatmap were plotted based on Euclidean distances and complete clustering.

## 3 Results

### 3.1 Sample collection

In order to examine how the metabolome of *S. meliloti* changes throughout a growth curve and to make comparisons between strains, we sampled the strains at 5 time points in M9 (four across the exponential phase, one at early stationary phase) and 3 time points in LBmc (mid-exponential phase, early stationary phase, and late stationary phase) (Fig. 1). Previous work has shown that the wild type, ΔpSymA, ΔpSymB, and ΔpSymAB strains display unique growth profiles; in minimal M9 medium the growth rate of each is distinct, while in complex LBmc medium the growth rate and maximal cell density differ (diCenzo et al. 2014). To account for the differences in growth rate, M9 cultures were sampled at pre-defined densities as opposed to pre-defined time points, as shown in the growth curves in Fig. 1a. As growth rate and entrance into stationary phase differ between the strains in LBmc, the time and density at sampling for each strain varied to ensure each culture was in the desired growth phase (Fig. 1b).

### 3.2 Metabolite analysis, feature detection, and quality control

For each sample, the intracellular or extracellular metabolic profiles were analyzed using LC–HILIC–TOF–MS as described in the Materials and Methods. A total of 3594 intracellular and 4081 extracellular metabolite features were initially identified using XCMS and CAMERA, each with a unique retention time and *m/z* value. 1474 intracellular and 2008 extracellular metabolite features remained after data processing and reduction, of which 1237 and 820 showed statistically significant changes between samples (Online Resource 1 Table S1). In some cases, a single metabolite can have multiple unique features corresponding to adducts or in-source fragment ions. Using authentic standards and MS/MS, 142 intracellular features were identified. These consisted of 49 lipids and 73 polar metabolites. Of 77 extracellular features that were identified, 2 were lipids and 65 were polar metabolites.

The extraction efficiency was 73–85 % and the biological variation was 18–29 % for the intracellular metabolome, and 12–26 % for the extracellular metabolome (Online Resource 1 Table S2). OPLS-DA was performed to assess the instrumentation reproducibility of the data by analyzing the variation of pooled samples. The pooled samples from intracellular or extracellular extracts were tightly clustered on the loading plots, which indicated that the technical variability was minimal in comparison to the biological variance of the experimental conditions (Online Resource 1 Figs. S1, S2).

### 3.3 Intracellular metabolic profiles of *S. meliloti* strains cultured in M9 minimal medium

To understand the contribution of pSymA and pSymB to the metabolism of *S. meliloti*, the intracellular metabolome

was analyzed at five time points across the growth curve of strains with or without pSymA and/or pSymB grown in a defined, minimal medium (M9). The global relationship between the samples was investigated using a supervised multivariate analysis (OPLS-DA) and a HCA (Fig. 2a, b). These global comparisons revealed clear metabolic shifts between strains and across time, and that the biological replicates for each sample clustered tightly together (Online Resource 1 Figs. S3, S4, Table S3). The presence/absence of pSymB was the major contributor to these metabolic differences, while the presence/absence of pSymA had a modest impact on the metabolome. These analyses also revealed that the metabolome of each strain was distinct at each of the five time points, although growth phase was the smallest contributor to the metabolic differences observed in this study. In general, the metabolome for all strains showed a progressive trend from the earliest (M1) to the latest (M5) time point (Online Resource 1 Fig. S3). However, whereas the greatest metabolic shift observed for the wild type, ΔpSymA, and ΔpSymAB occurred when cells transitioned from the exponential phase (M4) to stationary phase (M5), the largest metabolic disparity for ΔpSymB was observed early in the growth curve, between M1 and M2.

### 3.4 Metabolites contributing to the intracellular metabolic profile changes

Between subjects two-way ANOVA were performed to find the biomarker metabolite features that were primarily responsible for differences between strains and between growth phases as indicate through the OPLS-DA analysis. A HCA and fold-change heat map of the 1237 features with a $p$ value less than 0.01 as determined with a two-way ANOVA is shown in Fig. 2, and a similar plot showing the 100 most significantly changed features is presented in Online Resource 1 Fig. S5. While the chemical identities of few of the metabolites are known, the top 100 significantly changed metabolites include several sugars (galactose, sucrose), glutamic acid, glutamyl-hydroxyproline, and phosphatidylglycerol (PG) 35:2.

In examining just the identified intracellular polar metabolites, three notable groups of metabolites were observed (Fig. 3). Multiple sugar metabolites including sucrose, galactose, maltose, glucose, and trehalose were more abundant in the ΔpSymB and ΔpSymAB strains compared to the wild type and ΔpSymA. Increases associated with the loss of pSymB were also observed in many nucleotides and related compounds. Adenine, adenosine, inosine, 2-deoxyadenosine, guanine, and deoxyinosine were present in more abundance in the ΔpSymB and ΔpSymAB strains. Moreover, a purine breakdown product, hypoxanthine, was elevated in the stationary phase of all cultures, but remained high and steadily increased throughout the exponential phase of strains lacking pSymB, whereas the concentration in exponential phase was much lower in strains possessing pSymB. Finally, a number of amino acids (tyrosine, arginine, lysine, leucine, and glutamine) were elevated in the ΔpSymB and ΔpSymAB strains relative to the wild-type and the ΔpSymA strain. Serine and glutamate, on the hand, were elevated in the ΔpSymA and ΔpSymAB strains.

There were 49 phospholipids identified in the intracellular metabolome including 12 phosphatidylcholines (PC), 13 phosphatidylglycerols (PG), 21 phosphatidylethanolamines (PE) and 2 phosphatidic acids (PA). Of these 49, 17 were odd-chain phospholipids (cyclopropane-containing lipids) and 31 were even-chain phospholipids (Fig. 2d). ΔpSymB and ΔpSymAB had greater levels of odd-chain PCs, PGs, PE33:1 and PE33:2 compared to wild type and ΔpSymA. The remaining odd-chain PEs were less different between strains. Similarly, a greater abundance of even short-chain PCs including PC32:1 and PC34:1 were noted for ΔpSymB and ΔpSymAB in comparison to wild type and ΔpSymA. PG34:0, PG34:1, PG36:0 and PG36:2 were more abundant in pSymA-cured strains. No disparities in the other phospholipid classes were obvious between strains. A full list of identified intracellular metabolites and their relative abundances is included in the supplementary data (Online Resource 2).

### 3.5 Extracellular metabolic profiles of *S. meliloti* strains cultured in complex LBmc medium

We wished to evaluate the contribution of pSymA and pSymB towards the utilization of various metabolites in a nutritionally complex environment and to examine how *S. meliloti* influences its surrounding environment. To accomplish this, we employed a non-targeted approach by analyzing the composition of LBmc medium before and after growth of the four *S. meliloti* strains. LBmc is a complex medium containing carbohydrates, amino acids, peptide fragments, nucleotides, vitamins and other metabolites from casein hydrolysate and yeast extract. The uptake and metabolism of metabolites will remove them from the medium, whereas metabolites that require pSymA or pSymB for their utilization will not be removed from the medium by strains lacking these replicons. In addition, metabolites that are excreted from *S. meliloti* can be detected.

Blank LBmc, and spent LBmc from mid-exponential phase, as well as early and late stationary phase were analyzed. These extracellular metabolomes were assessed for global relationships using OPLS-DA and HCA (Fig. 4a, b). The 45 h inbucation of LBmc at 30 °C did not change the metabolite profile of the medium (Fig. 4), confirming

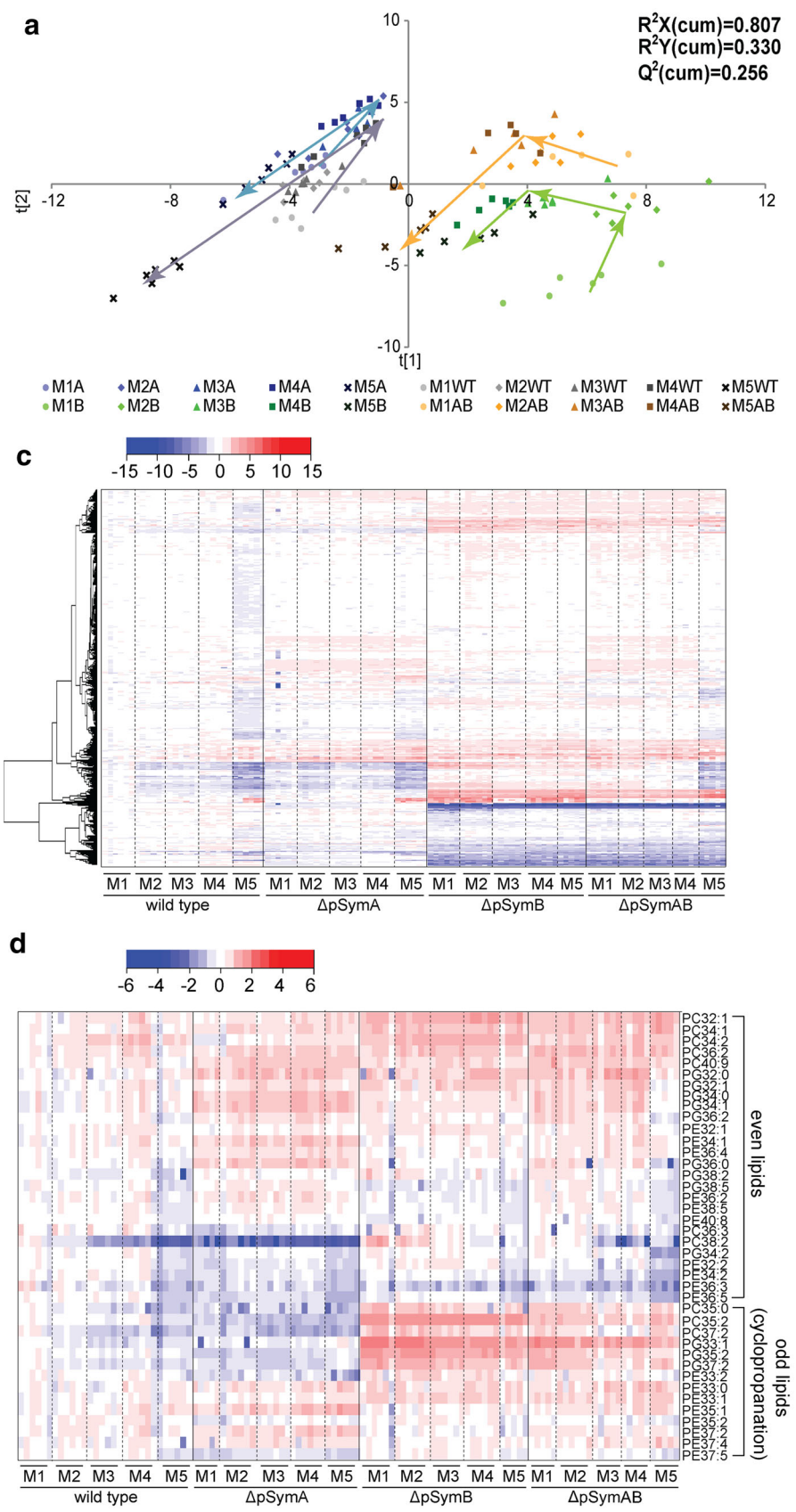
a
R²X(cum)=0.807
R²Y(cum)=0.330
Q²(cum)=0.256
t[1]
t[2]
M1A M2A M3A M4A M5A M1WT M2WT M3WT M4WT M5WT
M1B M2B M3B M4B M5B M1AB M2AB M3AB M4AB M5AB
b
c
-15 -10 -5 0 5 10 15
M1 M2 M3 M4 M5
wild type
ΔpSymA
ΔpSymB
ΔpSymAB
d
-6 -4 -2 0 2 4 6
even lipids
odd lipids (cyclopropanation)
35 30 25 20 15 10 5 0

◀**Fig. 2** Statistical analyses of the intracellular metabolome of wild-type, ΔpSymA, ΔpSymB, and ΔpSymAB *S. meliloti* at various growth phases including exponential phase (*M1–4*) and stationary phase (*M5*). **a** The OPLS-DA score plot showing the global relationship between the four *S. meliloti* strains at various growth phases, based on the 1474 detected metabolite features. Metabolome variance between strains and during growth was summarized by the x- and y-axes. The progression of growth is indicated by the *arrow* direction. The predictive statistic for the model fell below 0.4 ($Q^2 = 0.256$) due to similar metabolic profiles between strains and growth phases. **b** Heatmap of the 1237 significant metabolite features (between subject two-way ANOVA with Bonferroni correction, $p < 0.01$) plotted based on $\log_2$(fold change) with respect to the average metabolite levels in M1WT. **c** Heatmap of 41 significant phospholipids (between subject two-way ANOVA with Bonferroni correction, $p < 0.01$) plotted based on $\log_2$(fold change) with respect to the average metabolite levels in M1WT. M1A sample c (M1A-c) was removed as an outlier. **d** Hierarchical clustering analysis of the total detectable features (1474 features) for all four strains at each growth stage. *Black* wild type; *blue* ΔpSymA; *green* ΔpSymB; *orange* ΔpSymAB. *M1 circle*; *M2 diamond*; *M3 triangle*; *M4 square*; *M5 cross*. *WT* wild type; *A* ΔpSymA; *B* ΔpSymB; *AB* ΔpSymAB (Color figure online)

that any changes observed are a direct result of the growth of *S. meliloti*. The data for the biological replicates at each time point showed tight clustering, indicative of high reproducibility (Online Resource 1 Fig. S6, Table S4). As expected, samples from the mid-exponential phase cultures (L1) were most similar to the un-inoculated LBmc medium, whereas major changes in the extracellular metabolic profile were evident at L2 and L3 (Fig. 4c). Even though the wild-type and ΔpSymA samples at each time point clustered separately, the samples were quite similar throughout the growth curve but were distinctly different from the ΔpSymB and ΔpSymAB extracellular metabolic profiles. This trend was similar to that noted above for the intracellular metabolites.

### 3.6 Metabolites contributing to the extracellular metabolic profile changes

Of the 2008 extracellular metabolic features identified, 820 (~41 %) showed statistically significant changes between samples and the LBmc control (Fig. 4c). The majority of these were features that decreased throughout the growth curve of the wild type and ΔpSymA. Many, but by no means all, of these features also decreased in the spent media of ΔpSymB and ΔpSymAB cultures, although the decreases were often less dramatic. A heatmap showing the top 100 most significantly changed features is presented in Online Resource 1 Fig. S7. The top 100 significantly changed metabolites include amino acids and derivatives (ala-leu, met-ala, arginine, lysine, ornithine), nucleobases and nucleosides (adenine, adenosine, guanine, guanosine), maltose, and 2-phenylglycine. Of the 65 identified polar metabolites, compounds showing some level of decrease in all cultures included, but was not limited to, dipeptides (met-ala, ala-his, and ala-leu) and nucleotides and related compounds (guanosine, inosine, adenosine, and adenine), whereas many amino acids (arginine, ornithine, proline, glutamic acid, histidine, and serine) only decreased in the wild type and ΔpSymA (Fig. 5). No metabolites decreased only in strains lacking pSymA and/or pSymB.

Overall, there were a smaller percentage of features that showed an increase throughout the growth curves, and such changes were reduced when either pSymA and/or pSymB were removed from the genome (Fig. 5). Looking at the 61 identified polar metabolites, metabolites such as *N*-acetyl-glutamic acid, pantothenic acid, and nicotinic acid built up to some degree in the supernatant of all strains, whereas metabolites including *N*-acetyl-phenylalanine, sedoheptulosan, *N*-acetyl-glucosamine (GlcNAc), and citrulline only accumulated in the supernatant of the wild type and ΔpSymA. Interestingly, few metabolites only accumulated in the supernatant of strains lacking either pSymA and/or pSymB. Guanine, allantoin, arabitol, and malic acid accumulated only in the supernatant of the ΔpSymB and ΔpSymAB strains. Malic acid was particularly interesting; whereas malic acid was depleted from the media of wild-type and ΔpSymA cultures, malic acid accumulated more than tenfold in the ΔpSymB and ΔpSymAB cultures. A full list of identified extracellular metabolites and their relative abundances is included in the supplementary data (Online Resource 3).

## 4 Discussion

As the metabolic capabilities of the four strains examined in this study differ greatly (diCenzo et al. 2014), we chose to examine the intracellular metabolome of cultures grown in sucrose minimal medium to ensure all strains were utilizing the same compounds to support growth. Few metabolites showed large fold-changes across the exponential growth phase (M1–M4). However, a global decrease following the transition to the stationary phase (M5) was observed, consistent with a general repression of cellular metabolism following the cessation of growth (Chang et al. 2002). The sole exception was the ΔpSymB culture, suggesting that this culture had not fully entered stationary phase at the M5 time point. Larger magnitude changes were observed when comparing the metabolome between strains. The effect of pSymA and pSymB removal was starkly different (Fig. 2). The removal of pSymA had a relatively minor impact on the metabolome, with only a few metabolic features showing small increases in feature abundance. In contrast, the loss of pSymB resulted in many more metabolite features showing changes in abundance,

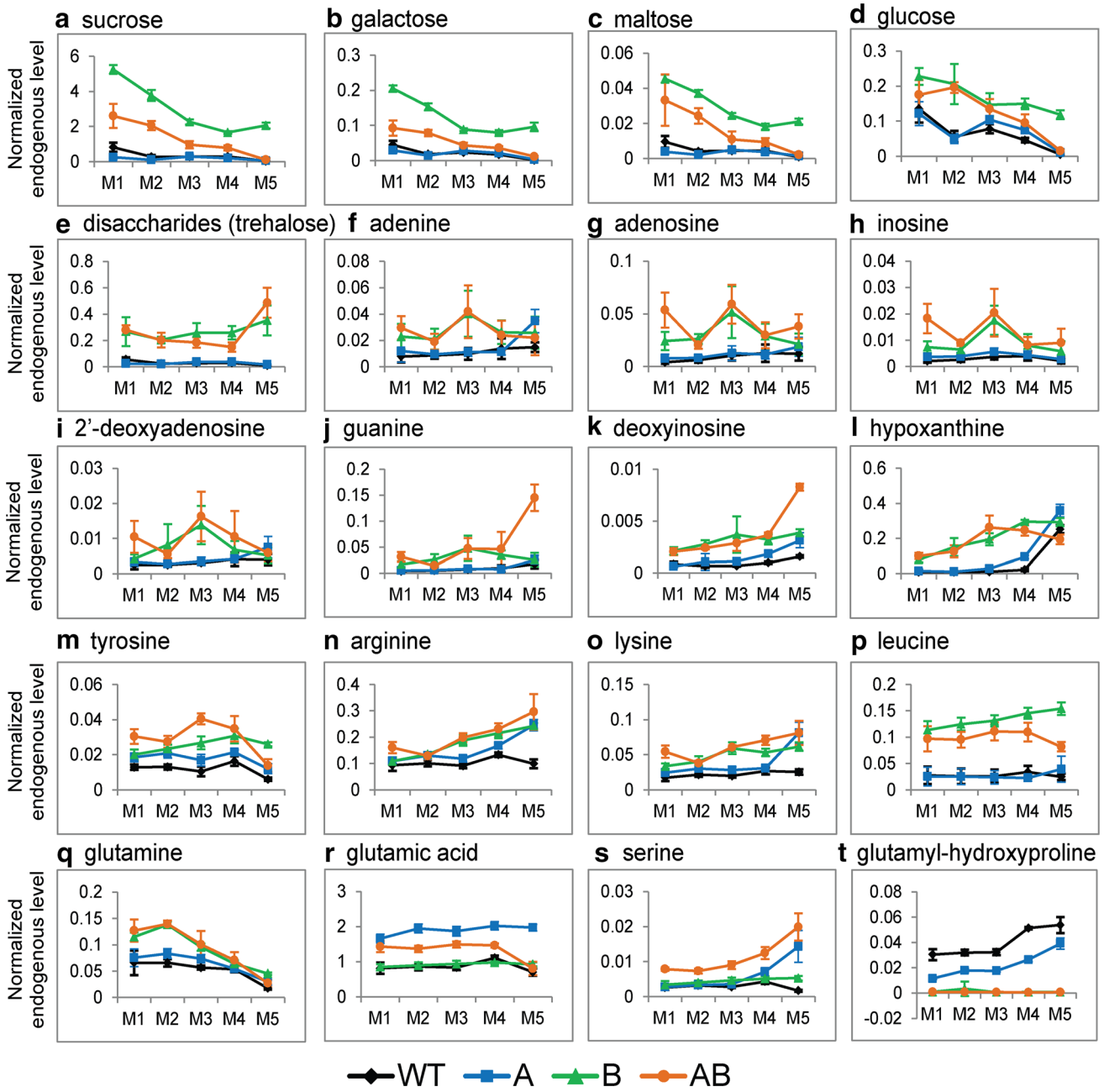


**Fig. 3** Intracellular levels of selected metabolites (**a–t**). Intracellular data were obtained from wild-type, ΔpSymA, ΔpSymB, and ΔpSymAB *S. meliloti* strains cultured in minimal M9 medium at 5 time points. n = 5–6. *Black* wild type; *blue* ΔpSymA; *green* ΔpSymB; *orange* ΔpSymAB. *M1–4* exponential phase; *M5* stationary phase; *error bar* represents two standard deviation (Color figure online)

with much greater fold changes, and with both increases and decreases in the metabolic features apparent.

Evolutionarily, pSymB is a much older addition to the *S. meliloti* genome than is pSymA, meaning pSymB has co-evolved with the core chromosome for a greater length of time (Galibert et al. 2001; Wong et al. 2002). Additionally, whereas the gene content of pSymA is highly variable between wild-type *S. meliloti* isolates, the composition of pSymB is strongly conserved (Epstein et al. 2012; Galardini et al. 2013; Guo et al. 2009). These observations, together with earlier work characterizing the phenotypic impact of the loss of pSymA and pSymB (diCenzo et al. 2014), have led to the suggestion that pSymA is an accessory replicon, largely specific to symbiosis and involved in adaptation to unique environments (diCenzo et al. 2014; Galardini et al. 2013). This is consistent with a proteomics study that identified only a few proteins present in free-living wild-type *S. meliloti* Rm2011 but absent in

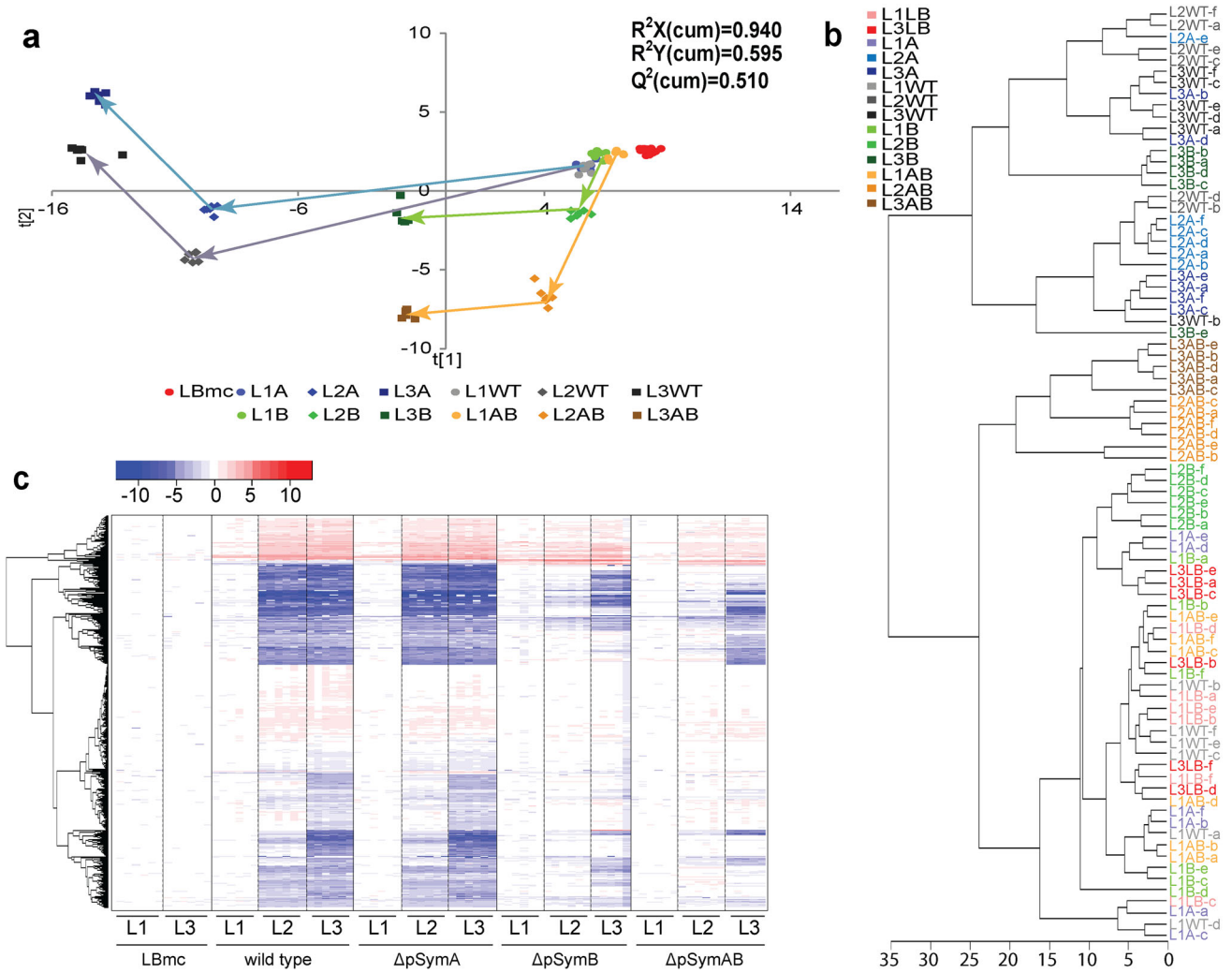


**Fig. 4** Statistical analyses of the extracellular metabolome of wild-type, ΔpSymA, ΔpSymB, and ΔpSymAB *S. meliloti* at various growth phases including mid-exponential phase (*L1*), early stationary phase (*L2*) and late stationary phase (*L3*) cultured in LBmc. **a** The OPLS-DA score plot showing the global relationship between the four strains of *S. meliloti* at various growth phases, based on the 2008 detected metabolite features. The progression of growth is indicated by the *arrow* direction. Metabolome variance between strains and during growth was summarized by the x- and y-axes. **b** Heatmap of the 820 significant metabolite features (between subject two-way ANOVA with Bonferroni correction, $p < 0.01$) plotted based on $\log_2$(fold change) with respect to the average metabolite levels in LBmc. **c** Hierarchical clustering analysis of the total detectable features (2008 features) for all four strains at each growth stage. LBmc *red*; *black* wild type; *blue* ΔpSymA; *green* ΔpSymB; *orange* ΔpSymAB. L1 *circle*; L2 *diamond*; L3 *square*. *WT* wild type; *A* ΔpSymA; *B* ΔpSymB; *AB* ΔpSymAB; *LBmc* LBmc blank following 0 and 45 h incubation at 30 °C (Color figure online)

ΔpSymA (Chen et al. 2000); in the free-living cell, pSymA is largely silent. In contrast, pSymB, while likely specialized for a particular niche (diCenzo et al. 2014; Galardini et al. 2013), has been more integrated into the core genome (Galardini et al. 2015). The metabolomics data presented here are consistent with these arguments. The loss of pSymA had a relatively modest impact on the metabolome of *S. meliloti*, and the accumulation of few, if any, metabolites appeared dependent on pSymA. On the other hand, removal of pSymB resulted in some drastic changes in abundance of metabolic features. Yet, ΔpSymAB grew quite well in the minimal medium considering nearly half the genome was removed. This would suggest that the metabolites whose synthesis are dependent on pSymB are predominately accessory metabolites.

It seems likely that many of the metabolites that accumulate in the ΔpSymB and ΔpSymAB strains were the result of the decreased growth rate of these strains and not directly linked to the absence of pSymB. The increased metabolites include several sugars, amino acids, and nucleotides and related compounds (Fig. 3). Presumably the abundances of these compounds reflect a steady state level established by the relative rate of their synthesis/uptake and their catabolism or incorporation into the

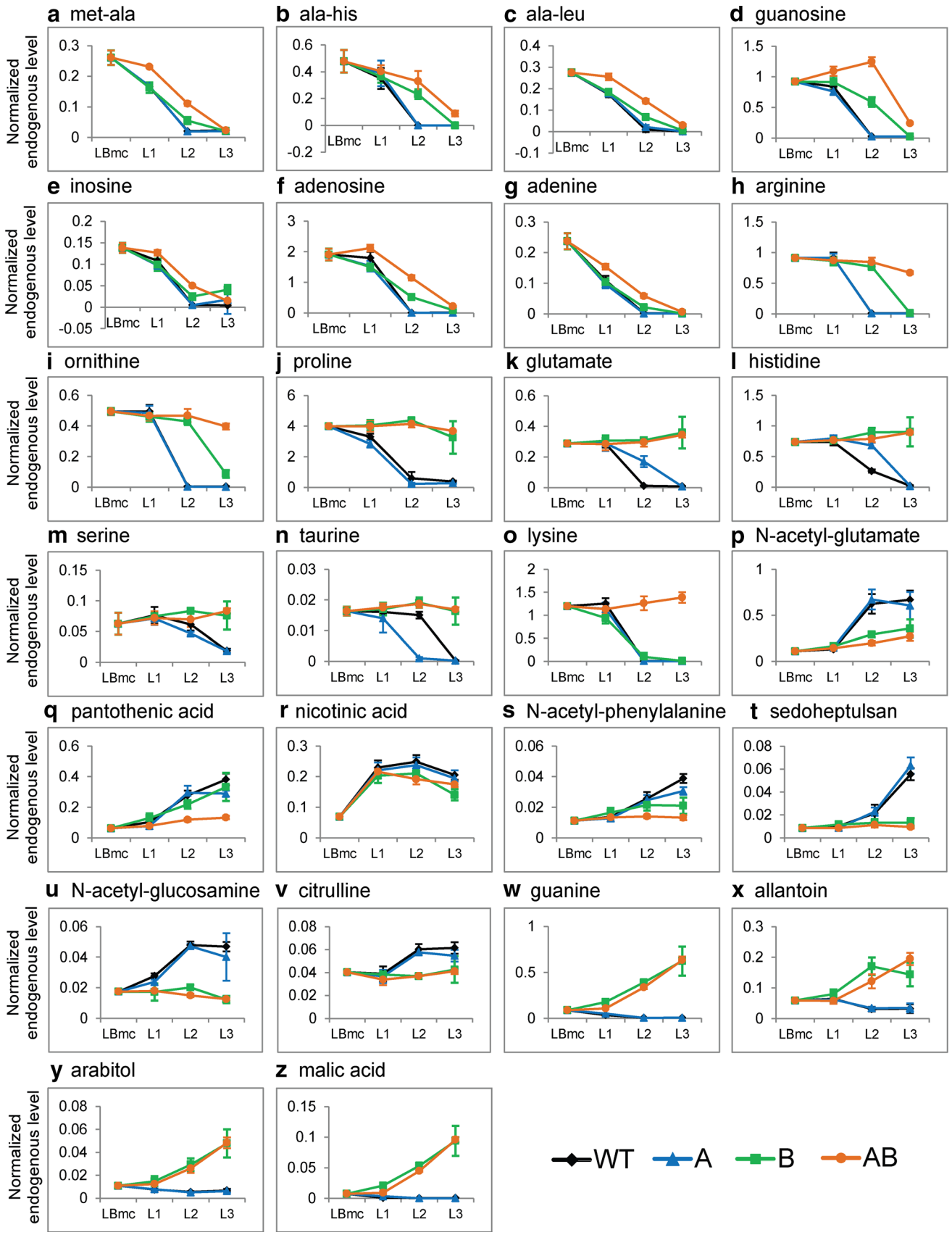
a met-ala
b ala-his
c ala-leu
d guanosine
e inosine
f adenosine
g adenine
h arginine
i ornithine
j proline
k glutamate
l histidine
m serine
n taurine
o lysine
p N-acetyl-glutamate
q pantothenic acid
r nicotinic acid
s N-acetyl-phenylalanine
t sedoheptulsan
u N-acetyl-glucosamine
v citrulline
w guanine
x allantoin
y arabitol
z malic acid
Normalized endogenous level
LBmc L1 L2 L3
WT A B AB

◀**Fig. 5** Extracellular data were obtained from various growth phases of wild-type, ΔpSymA, ΔpSymB, and ΔpSymAB *S. meliloti* strains cultured in LBmc medium (**a–z**). *Black* wildtype; *blue* ΔpSymA; *green* ΔpSymB; *orange* ΔpSymAB. *L1* mid-exponential phase; *L2* early stationary phase; *L3* late stationary phase, *LBmc* average of the readouts of 0 and 45 h LBmc blank at 30 °C; *error bar* represents two standard deviation (Color figure online)

appropriate macromolecules. Given that ΔpSymB and ΔpSymAB display a reduced growth rate relative to Rm2011, the rate that sugar is catabolized and the rate that nucleotides and amino acids are incorporated into nucleic acids and proteins is expected to decrease. If there is not a proportional decrease in the rate of uptake/synthesis of these compounds, their steady state level would increase, as is observed in this study.

Metabolites whose concentration decreased following the removal of pSymB (Fig. 2c) presumably reflect metabolites whose synthesis is pSymB dependent. While we are currently unable to explain most of the decreases, the pattern of hypoxanthine accumulation is notable as it helps validate our results. It has previously been shown that there is an intracellular accumulation of hypoxanthine in stationary phase cultures of *Escherichia coli* due to rRNA degradation (Rinas et al. 1995), and the hypoxanthine degradation genes are situated on pSymB in *S. meliloti* (Finan et al. 2001; Sukdeo and Charles 2003). The concentration of hypoxanthine in Rm2011 and ΔpSymA was elevated in stationary phase (M5) (Fig. 3i). In contrast, the concentration of hypoxanthine was elevated throughout the growth curve of ΔpSymB and ΔpSymAB with a modest increase with time, consistent with the inability of these strains to break down the hypoxanthine once sub-cultured and growth is re-initiated. The ability to correlate genomic and published data with the pattern of hypoxanthine accumulation in our data provides some evidence that the intracellular changes observed in this study are true changes.

The use of HILIC–TOF–MS allowed us to not only detect polar metabolites, but to also simultaneously monitor non-polar metabolites (Fei et al. 2014). Overall, the lipid composition noted here (Fig. 2d) was consistent with previous published results using GC–MS and ESI–MS/MS (Saborido Basconcillo et al. 2009). In comparing the lipid composition of the four strains, we observed that the relative composition of the different classes of phospholipids remained consistent between strains. However, several cyclopropanated lipids were present at higher levels in strains lacking pSymB. The cyclopropane bond is more stable than a double bound, and cyclopropanated-PL is known to increase *E. coli* resistance to acid stress and temperature shock (Zhang and Rock 2008). Increased cycloporpanation has also been correlated with acidic conditions and phosphate limitation in *S. meliloti* (Saborido Basconcillo et al. 2009). As pSymB is involved in osmoadaptation and exopolysaccharide biosynthesis (Dominguez-Ferreras et al. 2006; Finan et al. 2001, 1986), the removal of pSymB may have resulted in increased stress, including osmotic stress, resulting in increased lipid cyclopropanation.

Examining the extracellular metabolome of *S. meliloti* in complex LBmc medium facilitated an examination of the metabolic capacity and preferences of *S. meliloti*, how *S. meliloti* influences its environment, and how pSymA and pSymB contribute to these processes. It was expected that the removal of compounds from the medium would show a hierarchal usage with the most preferential compounds utilized first. The concentration of individual metabolites in LB can vary, but always the amino acids such as glutamic acid (11 mM), proline (9 mM), lysine (6 mM), leucine (8 mM), threonine (4 mM) and histidine (1 mM) are present at high concentrations relative to sugars such as glucose (0.1 mM) (Sezonov et al. 2007). It is striking that very few metabolites were completely removed by the wild-type or ΔpSymA strain by the time the populations reached a density of $2 \times 10^9$ CFU/mL ($OD_{600}$ of 1, i.e. time point L1) (Fig. 4c). As a cell density ($OD_{600}$) of 1 would normally require the catabolism of the equivalent of ~7 mM glucose (Osteras et al. 1995), the extracellular metabolite profile data indicated that many of the amino acids and other compounds were simultaneously metabolized. Nevertheless, a hierarchical usage was observed as a number of metabolic features were fully depleted by L2 (presumably the preferred nutrient sources), whereas others were not removed until L3.

Currently, Phenotype MicroArray™ (Biolog Inc) are the primary method to examine the metabolic capabilities of an organism by testing if an organism can individually metabolize or not a range of substrate; however, no insight is gained about the metabolic preferences of the organism. We show here that HILIC–TOF–MS allows us to detect the preferential usage of substrates in a nutritionally complex environment, and thus will be a valuable technique to complement Phenotype MicroArray™ studies. Additionally, this technique has potential in examining the metabolism of an organism in complex, environmental samples. For example, the nutritional environment of *S. meliloti* in the rhizosphere is generally accepted to be highly influenced by plant root exudates. By growing *S. meliloti* in a medium containing purified plant root exudate as the carbon source, HILIC–TOF–MS would allow the detection of which root exudates are utilized by *S. meliloti*, and the preference of *S. meliloti* for these different compounds.

Cross-strain comparisons revealed the exometabolome of Rm2011 and ΔpSymA were highly similar (Fig. 4), consistent with this replicon being involved in the

catabolism of few substrates (diCenzo et al. 2014; Oresnik et al. 2000). On the other hand, previous work has implicated pSymB in the transport and catabolism of a broad range of substrates, particularly carbon sources (diCenzo et al. 2014; Finan et al. 2001; Mauchline et al. 2006), and indeed, many substrates that are removed from the medium by the wild type remain in the spent media of ΔpSymAB cultures (Fig. 4c). Many of the organic acids, several of which are relevant during symbiosis (Dunn 2014), fall into this category, including serine, lysine, arginine, ornithine, proline, histidine, and taurine (Fig. 5h, i, j, l, m, n, o). For histidine, taurine, ornithine, and likely arginine, this is due to the presence of the corresponding catabolic genes on pSymB, and at least in the case or taurine, the transport genes as well (diCenzo et al. 2015; Dunn 2014; Finan et al. 2001; Mostafavi et al. 2014). Though ΔpSymAB did not utilize arginine or proline, the ability of exogenous arginine and proline to complement ΔpSymAB arginine and proline auxotrophs (diCenzo and Finan 2015), respectively, indicate that the ΔpSymAB strain can transport these amino acids (data not shown). Intriguingly, lysine was not metabolized only by the ΔpSymAB strain, suggestive of functional redundancy in lysine transport or metabolism, a common phenomenon in *S. meliloti* (diCenzo and Finan 2015).

The ΔpSymB and ΔpSymAB strains enter stationary phase at a density greater than five-fold less than the wild type and ΔpSymA (Fig. 1b). As Phenotype MicroArray™ studies indicated that these two strains are unable to utilize more than half the carbon sources, including most amino acids, that can be used by the wild type, it was suggested that the reduced density in LBmc was a result of carbon starvation (diCenzo et al. 2014). The work here shows that the ΔpSymB and ΔpSymAB strains are indeed highly impaired in their ability to utilize amino acids as a carbon source, as they remain at a high concentration even following the onset of stationary phase (Fig. 5). Furthermore, adding sucrose to LBmc allows the ΔpSymB and ΔpSymAB strains to reach a higher cell density, consistent the cessation of growth corresponding to carbon starvation (data not shown). As amino acids and oligopeptides are the primary carbon source in LBmc (Sezonov et al. 2007), these observations indicate that the reduced stationary phase density of the ΔpSymB and ΔpSymAB strains is a result of an inability to metabolize the amino acids as a carbon source.

A number of extracellular metabolic features increased in the medium following growth of all four strains, but perhaps more interesting are those that only increased when pSymB was absent. These compounds may represent products of pathways that are incomplete because of the absence of the pSymB replicon. Alternatively, as a part of normal cellular metabolism, some compounds may always be produced, secreted, and subsequently re-assimilated and metabolized by *S. meliloti*. But if the necessary uptake transporter were encoded by pSymB, these compounds would be unable to be re-assimilated in the ΔpSymB and ΔpSymAB strains. For example, *S. meliloti* has previously been observed to secrete, and then re-assimilate, malate (Carson et al. 1992). However, the $C_4$-dicarboxylate transport system encoded by *dctA* is located on the pSymB replicon (Finan et al. 1988; Watson et al. 1988). Hence, unlike the wild type, ΔpSymB and ΔpSymAB are unable to re-assimilate the secreted malate, resulting in its accumulation in the medium (Fig. 5z).

In conclusion, the analysis of intracellular and extracellular metabolites from the *S. meliloti* cultures lead to interesting insights with respect to these strains and particularly the catabolic functions for genes of the pSymB replicon. For future studies employing extracellular profiling, the inclusion of a media containing known concentrations of amino acids and nucleotides would offer advantages in the analysis of the data.

**Acknowledgments** This work is dedicated to the late Prof. Brian McCarry (1946–2013). Funding for this work was provided by NSERC to B. E. M. and T. M. F. The authors would like to thank the Center for Microbial Chemical Biology (CMCB) at McMaster for access to the LC–MS. F. F. is supported by an Ontario Graduate Scholarship and G. C. D by a NSERC CGS award.

**Compliance with ethical standards**

**Conflict of interest** Authors Fan Fei, George C. diCenzo, Dawn M. E. Bowdish, Brian E. McCarry (deceased), and Turlough M. Finan declare that they have no conflict of interest.

**Ethical Approval** This work did not involve human particpants and/or animals, and all authors have agreed to submission of the manuscript.

## References

Barsch, A., Patschkowski, T., & Niehaus, K. (2004). Comprehensive metabolite profiling of *Sinorhizobium meliloti* using gas chromatography-mass spectrometry. *Functional & Integrative Genomics, 4*(4), 219–230. doi:10.1007/s10142-004-0117-y.

Barsch, A., Tellström, V., Patschkowski, T., Küster, H., & Niehaus, K. (2006). Metabolite profiles of nodulated alfalfa plants indicate that distinct stages of nodule organogenesis are accompanied by global physiological adaptations. *Molecular Plant-Microbe Interactions, 19*(9), 998–1013. doi:10.1094/MPMI-19-0998.

Carson, K. C., Holliday, S., Glenn, A. R., & Dilworth, M. J. (1992). Siderophore and organic acid production in root nodule bacteria. *Archives of Microbiology, 157*, 264–271.

Chang, D.-E., Smalley, D. J., & Conway, T. (2002). Gene expression profiling of *Escherichia coli* growth transitions: an expanded stringent response model. *Molecular Microbiology, 45*(2), 289–306.

Chen, H., Higgins, J., Oresnik, I. J., Hynes, M. F., Natera, S., Djordjevic, M. A., et al. (2000). Proteome analysis demonstrates

complex replicon and luteolin interactions in pSyma-cured derivatives of *Sinorhizobium meliloti* strain 2011. *Electrophoresis, 21*, 3833–3842.

diCenzo, G. C., & Finan, T. M. (2015). Genetic redundancy is prevalent within the 6.7 Mb *Sinorhizobium meliloti* genome. *Molecular Genetics and Genomics, 290*(4), 1345–1356. doi:10.1007/s00438-015-0998-6.

diCenzo, G. C., MacLean, A. M., Milunovic, B., Golding, G. B., & Finan, T. M. (2014). Examination of prokaryotic multipartite genome evolution through experimental genome reduction. *PLoS Genetics, 10*(10), e1004742. doi:10.1371/journal.pgen.1004742.

diCenzo, G., Milunovic, B., Cheng, J., & Finan, T. M. (2013). The tRNAarg gene and *engA* are essential genes on the 1.7-mb pSymB megaplasmid of *Sinorhizobium meliloti* and were translocated together from the chromosome in an ancestral strain. *Journal of Bacteriology, 195*(2), 202–212. doi:10.1128/JB.01758-12.

diCenzo, G. C., Zamani, M., Cowie, A., & Finan, T. M. (2015). Proline auxotrophy in *Sinorhizobium meliloti* results in a plant-specific symbiotic phenotype. *Microbiology,*. doi:10.1099/mic.0.000182.

Dominguez-Ferreras, A., Perez-Arnedo, R., Becker, A., Olivares, J., Soto, M. J., & Sanjuan, J. (2006). transcriptome profiling reveals the importance of plasmid pSymB for Osmoadaptation of *Sinorhizobium meliloti*. *Journal of Bacteriology, 188*(21), 7617–7625. doi:10.1128/JB.00719-06.

Dunn, M. F. (2014). Key roles of microsymbiont amino acid metabolism in rhizobia-legume interactions. *Critical Reviews in Microbiology,*. doi:10.3109/1040841X.2013.856854.

Dunn, W. B., Broadhurst, D., Begley, P., Zelena, E., Francis-McIntyre, S., Anderson, N., et al. (2011). Procedures for large-scale metabolic profiling of serum and plasma using gas chromatography and liquid chromatography coupled to mass spectrometry. *Nature Protocols, 6*(7), 1060–1083. doi:10.1038/nprot.2011.335.

Epstein, B., Branca, A., Mudge, J., Bharti, A. K., Briskine, R., Farmer, A. D., et al. (2012). Population genomics of the facultatively mutualistic bacteria *Sinorhizobium meliloti* and *S. medicae*. *PLoS Genetics, 8*(8), e1002868. doi:10.1371/journal.pgen.1002868.

Fei, F., Bowdish, D. M. E., & McCarry, B. E. (2014). Comprehensive and simultaneous coverage of lipid and polar metabolites for endogenous cellular metabolomics using HILIC-TOF-MS. *Analytical and Bioanalytical Chemistry, 406*, 3723–3733. doi:10.1007/s00216-014-7797-5.

Finan, T. M., Kunkel, B., De Vos, G. F., & Signer, E. R. (1986). Second symbiotic megaplasmid in *Rhizobium meliloti* carrying exopolysaccharide and thiamine synthesis genes. *Journal of Bacteriology, 167*(1), 66–72.

Finan, T. M., O'Brian, M. R., Layzell, D. B., Vessey, J. K., & Newton, W. (Eds.). (2002). *Nitrogen fixation: Global perspectives*. Wallingford: CABI Publishing.

Finan, T. M., Oresnik, I. J., & Bottacin, A. (1988). Mutants of *Rhizobium meliloti* defective in succinate metabolism. *Journal of Bacteriology, 170*(8), 3396–3403.

Finan, T. M., Weidner, S., Wong, K., Buhrmester, J., Chain, P., Vorhölter, F. J., et al. (2001). The complete sequence of the 1683-kb pSymB megaplasmid from the $N_2$-fixing endosymbiont *Sinorhizobium meliloti*. *Proceedings of the National Academy of Sciences of the United States of America, 98*(17), 9889–9894. doi:10.1073/pnas.161294698.

Galardini, M., Brilli, M., Spini, G., Rossi, M., Roncaglia, B., Bani, A., et al. (2015). Evolution of intra-specific regulatory networks in a multipartite bacterial genome. *PLoS Computational Biology, 11*(9), e1004478. doi:10.1371/journal.pcbi.1004478.

Galardini, M., Pini, F., Bazzicalupo, M., Biondi, E. G., & Mengoni, A. (2013). Replicon-dependent bacterial genome evolution: the case of *Sinorhizobium meliloti*. *Genome Biology and Evolution, 5*(3), 542–558. doi:10.1093/gbe/evt027.

Galibert, F., Finan, T. M., Long, S. R., Pühler, A., Abola, A. P., Ampe, F., et al. (2001). The composite genome of the legume symbiont *Sinorhizobium meliloti*. *Science, 293*(5530), 668–672. doi:10.1126/science.1060966.

Geddes, B. A., & Oresnik, I. J. (2014). Physiology, genetics, and biochemistry of carbon metabolism in the alphaproteobacterium *Sinorhizobium meliloti*. *Canadian Journal of Microbiology, 60*(8), 491–507. doi:10.1139/cjm-2014-0306.

Gemperline, E., Jayaraman, D., Maeda, J., Ané, J.-M., & Li, L. (2015). Multifaceted investigation of metabolites during nitrogen fixation in *Medicago* via high resolution MALDI-MS imaging and ESI-MS. *Journal of the American Society for Mass Spectrometry, 26*(1), 149–158. doi:10.1007/s13361-014-1010-0.

Guo, H., Sun, S., Eardly, B., Finan, T., & Xu, J. (2009). Genome variation in the symbiotic nitrogen-fixing bacterium *Sinorhizobium meliloti*. *Genome, 52*(10), 862–875. doi:10.1139/G09-060.

Harrison, P. W., Lower, R. P. J., Kim, N. K. D., & Young, J. P. W. (2010). Introducing the bacterial "chromid": not a chromosome, not a plasmid. *Trends in Microbiology, 18*(4), 141–148. doi:10.1016/j.tim.2009.12.010.

Jonas, O. A. H., Spurgeon, D. J., Svendsen, C., & Griffin, J. L. (2008). A metabolomics based approach to assessing the toxicity of the polyaromatic hydrocarbon pyrene to the earthworm *Lumbricus rubellus*. *Chemosphere, 71*, 601–609. doi:10.1016/j.chemosphere.2007.08.056.

Keum, Y. S., Seo, J. S., Li, Q. X., & Kim, J. H. (2008). Comparative metabolomic analysis of *Sinorhizobium* sp. C4 during the degradation of phenanthrene. *Applied Microbiology and Biotechnology, 80*(5), 863–872. doi:10.1007/s00253-008-1581-4.

Krawiec, S., & Riley, M. (1990). Organization of the bacterial chromosome. *Microbiological Reviews, 54*(4), 502–539.

Kuhl, C., Tautenhahn, R., Böttcher, C., Larson, T. R., & Neumann, S. (2012). CAMERA: An integraged strategy for compound spectra extraction and annotation of LC/MS data sets. *Analytical Chemistry, 84*(1), 283–289. doi:10.1021/ac202450g.

Mauchline, T. H., Fowler, J. E., East, A. K., Sartor, A. L., Zaheer, R., Hosie, A. H. F., et al. (2006). Mapping the *Sinorhizobium meliloti* 1021 solute-binding protein-dependent transportome. *Proceedings of the National Academy of Sciences of the United States of America, 103*(47), 17933–17938. doi:10.1073/pnas.0606673103.

Mostafavi, M., Lewis, J. C., Saini, T., Bustamante, J. A., Gao, I. T., Tran, T. T., et al. (2014). Analysis of a taurine-dependent promoter in *Sinorhizobium meliloti* that offers tight modulation of gene expression. *BMC Microbiology, 14*(1), 295. doi:10.1186/s12866-014-0295-2.

Ong, L. C., & Lin, Y.-H. (2003). Metabolite profiles and growth characteristics of *Rhizobium meliloti* cultivated at different specific growth rates. *Biotechnology Progress, 19*(3), 714–719. doi:10.1021/bp025758w.

Oresnik, I. J., Liu, S. L., Yost, C. K., & Hynes, M. F. (2000). Megaplasmid pRme2011a of *Sinorhizobium meliloti* is not required for viability. *Journal of Bacteriology, 182*(12), 3582–3586.

Osteras, M., Driscoll, B. T., & Finan, T. M. (1995). Molecular and expression analysis of the *Rhizobium meliloti* phosphoenolpyruvate carboxykinase (*pckA*) gene. *Journal of Bacteriology, 177*(6), 1452–1460.

Rinas, U., Hellmuth, K., Kang, R., Seeger, A., & Schlieker, H. (1995). Entry of *Escherichia coli* into stationary phase is indicated by endogenous and exogenous accumulation of nucleobases. *Applied and Environmental Microbiology, 61*(12), 4147–4151.

Saborido Basconcillo, L., Zaheer, R., Finan, T. M., & McCarry, B. E. (2009). Cyclopropane fatty acyl synthase in *Sinorhizobium meliloti*. *Microbiology, 155*(Pt 2), 373–385. doi:10.1099/mic.0.022608-0.

Sallet, E., Roux, B., Sauviac, L., Jardinaud, M.-F., Carrère, S., Faraut, T., et al. (2013). Next-generation annotation of prokaryotic genomes with EuGene-P: application to *Sinorhizobium meliloti* 2011. *DNA Research, 20*(4), 339–354. doi:10.1093/dnares/dst014.

Sezonov, G., Joseleau-Petit, D., & D'Ari, R. (2007). *Escherichia coli* physiology in Luria-Bertani broth. *Journal of Bacteriology, 189*(23), 8746–8749. doi:10.1128/JB.01368-07.

Smith, C. A., O'Maille, G., Want, E. J., Qin, C., Trauger, S. A., Brandon, T. R., et al. (2005). METLIN: A metabolite mass spectral database. *Therapeutic Drug Monitoring, 27*(6), 747–751.

Smith, C. A., Want, E. J., O'Maille, G., Abagyan, R., & Siuzdak, G. (2006). XCMS: processing mass spectrometry data for metabolite profiling using nonlinear peak alignment, matching, and identification. *Analytical Chemistry, 78*, 779–787. doi:10.1021/ac051437y.

Sukdeo, N., & Charles, T. C. (2003). Application of crossover-PCR-mediated deletion-insertion mutagenesis to analysis of the *bdhA-xdhA2-xdhB2* mixed-function operon of *Sinorhizobium meliloti*. *Archives of Microbiology, 179*, 301–304. doi:10.1007/s00203-003-0532-9.

Watson, R. J., Chan, Y. K., Wheatcroft, R., Yang, A. F., & Han, S. H. (1988). *Rhizobium meliloti* genes required for $C_4$-dicarboxylate transport and symbiotic nitrogen fixation are located on a megaplasmid. *Journal of Bacteriology, 170*(2), 927–934.

Wong, K., Finan, T., & Golding, B. (2002). Dinucleotide compositional analysis of *Sinorhizobium meliloti* using the genome signature: distinguishing chromosomes and plasmids. *Functional & Integrative Genomics, 2*(6), 274–281. doi:10.1007/s10142-002-0068-0.

Xia, J., Sinelnikov, I. V., Han, B., & Wishart, D. S. (2015). MetaboAnalyst 3.0-making metabolomics more meaningful. *Nucleic Acids Research,*. doi:10.1093/nar/gkv380.

Ye, H., Gemperline, E., Venkateshwaran, M., Chen, R., Delaux, P.-M., Howes-Podoll, M., et al. (2013). MALDI mass spectrometry-assisted molecular imaging of metabolites during nitrogen fixation in the *Medicago truncatula-Sinorhizobium meliloti* symbiosis. *The Plant Journal, 75*(1), 130–145. doi:10.1111/tpj.12191.

Zhang, Y.-M., & Rock, C. O. (2008). Membrane lipid homeostasis in bacteria. *Nature Reviews Microbiology, 6*(3), 222–233. doi:10.1038/nrmicro1839.

Zhao, H., Li, M., Fang, K., Chen, W., & Wang, J. (2012). In silico insights into the symbiotic nitrogen fixation in *Sinorhizobium meliloti* via metabolic reconstruction. *PLoS One, 7*(2), e31287. doi:10.1371/journal.pone.0031287.